Aalto University

OPEN ACCESS

This is an electronic reprint of the original article.
This reprint may differ from the original in pagination and typographic detail.

Zitting, Aleksi; Paajanen, Antti; Altgen, Michael; Rautkari, Lauri; Penttilä, Paavo A.

Role of Lignin in Moisture Interactions of Cellulose Microfibril Structures in Wood

Published in:
Small Structures

DOI:
10.1002/sstr.202400167

Published: 01/12/2024

Document Version
Publisher's PDF, also known as Version of record

Published under the following license:
CC BY

Please cite the original version:
Zitting, A., Paajanen, A., Altgen, M., Rautkari, L., & Penttilä, P. A. (2024). Role of Lignin in Moisture Interactions of Cellulose Microfibril Structures in Wood. *Small Structures*, *5*(12), Article 2400167. https://doi.org/10.1002/sstr.202400167

This material is protected by copyright and other intellectual property rights, and duplication or sale of all or part of any of the repository collections is not permitted, except that material may be duplicated by you for your research use or educational purposes in electronic or print form. You must obtain permission for any other use. Electronic or print copies may not be offered, whether for sale or otherwise to anyone who is not an authorised user.

small structures
www.small-structures.com

Role of Lignin in Moisture Interactions of Cellulose Microfibril Structures in Wood

Aleksi Zitting, Antti Paajanen, Michael Altgen, Lauri Rautkari, and Paavo A. Penttilä**

Wood is a complex, multi-component material with a variety of applications. The properties of wood are especially sensitive to its moisture content and comprehending wood–water interactions is thus paramount. Understanding of the moisture interactions of the wood polysaccharide components, cellulose microfibrils and hemicelluloses, is improving. However, the role of lignin remains less clear. In this work, X-ray scattering measurements were carried out on delignified spruce undergoing a desorption-adsorption cycle, and the results were compared to previous data from untreated wood. In addition, a molecular model of the cell wall nanostructure, including the main chemical components, was used to support the experimental results. Based on the small-angle scattering, delignification affects the arrangement of cellulose microfibrils in the cell wall by increasing their packing distance. Wide-angle scattering shows that delignification has no substantial effect on the cellulose crystal structure and how it changes with moisture. Both the scattering results and simulations suggest that lignin is a passive, rather than an active participant in the moisture response of microfibril bundles in wood cell walls. Small-angle scattering from fully wet delignified wood reveals a contribution that can be assigned to aligned nanometer scale pores which close during drying.

1. Introduction

Wood is a complex and hierarchical natural material used in a broad range of applications. Many of its properties are fundamentally derived from the cell walls which comprise the bulk of wood. The properties of the cell walls are, in turn, largely determined by their structure in the 1–100 nm scale. Additionally, wood and essentially all its chemical components closely interact with water, since wood is a water transport and storage material of a living plant. The properties of wood are also largely affected by moisture, meaning that the interaction with water dictates the use of wood in most applications.[1,2]

The main chemical components of the wood cell wall are cellulose, which forms crystalline microfibrils, the shorter and branched hemicelluloses which surround the fibrils and can link with other cell wall components, and the amorphous lignin.[3] While the sorption of water is known to cause the swelling of cellulose microfibril bundles by the adsorption of water to the interfibrillar spaces occupied by hemicelluloses, the role of lignin is less clear.[4] Lignin is generally considered to be hydrophobic, at least relative to the other cell wall components, and likely is a less active participant in wood–water interactions. However, its presence in wood will at least passively affect the moisture behavior, as it takes up space that could possibly be taken up by water, affects the diffusion path length of water molecules, and possibly blocks access to the hydrophilic polysaccharide components.[5]

The chemical differences between lignin and the cell wall polysaccharides enable the application of chemical isolation techniques that selectively, albeit not entirely, target lignin while minimizing interference with cellulose and hemicelluloses. These chemical isolation methods might alter the lignin structure and morphology, so that analyzing the isolated lignin does not provide the full picture of its role inside the cell wall.[6] However, the relative easiness of removing lignin from wood presents an opportunity for indirect characterization of its role in the wood cell walls. It is possible to remove most of the lignin from a wood sample while trying to retain the rest of the structure, mainly the cellulose microfibrils and hemicelluloses. Characterizing wood where the lignin has been removed and comparing it to untreated wood allows inferring the role of lignin inside the wood cell wall.[7] The measured differences provide insights into the impact lignin has on the cell wall nanostructure and its moisture behavior, though the delignification method will have an impact itself. Additionally, delignified wood itself is an interesting research subject, since it is used in many applications or as a precursor when producing advanced wood materials such as densified or transparent wood.[8,9]

Studying the cell wall nanostructure and its moisture response is not straightforward since most characterization methods require sample preparation that at least partially destroys the cell wall. Scattering methods such as X-ray and neutron scattering

A. Zitting, M. Altgen, L. Rautkari, P. A. Penttilä
Department of Bioproducts and Biosystems
Aalto University
Vuorimiehentie 1, 02150 Espoo, Finland
E-mail: aleksi.zitting@aalto.fi; paavo.penttila@aalto.fi

A. Paajanen
VTT Technical Research Centre of Finland Ltd
Kivimiehentie 3, 02150 Espoo, Finland

The ORCID identification number(s) for the author(s) of this article can be found under https://doi.org/10.1002/sstr.202400167.

© 2024 The Author(s). Small Structures published by Wiley-VCH GmbH. This is an open access article under the terms of the Creative Commons Attribution License, which permits use, distribution and reproduction in any medium, provided the original work is properly cited.

DOI: 10.1002/sstr.202400167

allow for non-destructive characterization of the wood cell wall nanostructure.[10,11] Scattering methods are especially sensitive to the changes in the oriented, crystalline cellulose microfibrils due to their abundance and ordered structure. The two other cell wall components, hemicelluloses and lignin, are more difficult to analyze since they do not form crystalline fibril structures. This is especially true for lignin, which is an amorphous polymer.

However, interpreting the nanostructure using only scattering is both challenging and unlikely to provide the whole picture, particularly since the scattering contribution from hemicelluloses and lignin is hard to isolate. Molecular modeling of cellulose, hemicelluloses, and lignin enables the simulation of the cell wall components and their interactions with each other, and how the structures respond when water is added to or removed from the system. Using the models to study how lignin affects various nanoscale behaviors, including the spatial distribution of water, can provide information on the role of lignin and aid in interpreting the experimental scattering results and connecting them to changes in the cell wall.

The aim of this work is to investigate the role of lignin in the moisture behavior of wood cell walls by comparing experimental scattering results from untreated and delignified spruce samples. Molecular simulations are used to provide further details on the moisture response of both microfibril bundles and lignin. In particular, we aim to test the hypothesis of our previous work[4] that lignin is not directly involved in the fundamental moisture interactions of microfibrils in wood cell walls, and instead only passively affects fibril packing and moisture adsorption. In addition, we elucidate the structure and moisture behavior of delignified wood.

2. Experimental Section

2.1. Materials

Stem discs at around 1 m height from a freshly felled and mature Norway spruce (*Picea abies*) were sealed in plastic bags and stored at −20 °C. From these discs, sapwood blocks with a tangential width of roughly 1 cm were sawed using a handsaw. A sliding microtome (Lab-Microtome, Swiss Federal Research Institute WSL) was used to cut the wood blocks into ≈1 mm thick tangential-longitudinal sections. A razor blade was used to further cut the sections into $1 \times 1 \times 10\,mm^3$ (radial × tangential × longitudinal) pieces containing both earlywood and latewood.

The wood pieces were delignified using the acid chlorite method, as detailed by Schuerch.[12] This process typically preserves most of the hemicelluloses whilst significantly reducing lignin content.[13] Initially, the wood and 160 mL of deionized water were heated to 80 °C, and 0.5 mL of glacial acetic acid and 1.5 g of sodium chlorite were added. This addition was repeated at the 1, 2, and 3 h mark. After a total duration of 4 h, the wood pieces were removed from the solution, rinsed with deionized water, and stored in deionized water to ensure they remained in a fully wet state.

2.2. Confocal Raman Mapping

Successful delignification of the samples was confirmed using confocal Raman mapping. Transversal sections with a thickness of ≈20 µm were cut from untreated and delignified spruce wood with a rotary microtome (Nahita ZFP-011). The sections were placed on glass slides together with a droplet of deionized water, covered with a glass coverslip (thickness 0.17 mm), and sealed with nail polish. Images were collected using a Renishaw InVia Qontor confocal Raman microscope equipped with a 532 nm diode laser and a Centrus 05TJ55 CCD detector behind an 830 lines per mm grating. The measurements were conducted within the spectral range between 97 and 3667 cm^{-1} using an integration time of 0.2 s and either a 20× air objective (NA 0.4) or a 63× water objective (NA 1.2). Images collected with the 20× air objective contained 220 lines per image and 220 points per line at a step size of 0.5 µm. Images collected with the 63× water objective contained 225 lines per images and 225 points per line at a step size of 0.2 µm. Raman images were generated after cosmic ray removal by area integration in the wavenumber range of 1550–1700 cm^{-1}. Average spectra were extracted from the cell wall and cell corner regions of images taken with the 63× objective. The spectra were baseline corrected by fitting a 9th order polynomial but not normalized.

2.3. X-ray Scattering

2.3.1. X-ray Scattering Measurements

To measure delignified wood in the water-saturated state, the sample was removed from the deionized water, wrapped in Mylar foil and placed in a humidity chamber with controlled humidity and temperature (Xenocs). The windows of the chamber were Kapton foil. The relative humidity (RH) was set to 95% and temperature to 25 °C. The sample was oriented so that the fiber axis was vertical and perpendicular to the X-ray beam. Small and wide-angle X-ray scattering (SAXS, WAXS) were measured using Xenocs Xeuss 3.0C equipped with a GeniX 3D Cu-source (wavelength $\lambda = 1.542$ Å) and an EIGER2 R 1 M detector. WAXS data was collected at a sample-to-detector distance of 150 mm. Line eraser mode was used to remove gaps from the scattering patterns, and virtual detector mode was used to produce 12 images per measurement and to cover the q-range of –0.05–2.5 $Å^{-1}$ (scattering vector $q = \frac{4\pi \sin(\theta)}{\lambda}$ with scattering angle 2θ). Acquisition time for each single image was 500 s. SAXS data was taken at a sample-to-detector distance of 1000 mm using the line eraser mode with each single image taking 300 s. The SAXS measurements covered a q-range of $0.02 - 0.25\,Å^{-1}$. Background for the water-saturated sample was measured from Mylar foil in the humidity chamber. After measuring the water-saturated sample, the Mylar was removed and the sample was left to equilibrate in the chamber at RH 95% for roughly 18 h. RH was varied first with a desorption cycle with steps of 95%, 85%, 70%, 50%, 20%, 10% and then with an adsorption cycle going back up with the steps 20%, 50%, 70%, 85%, and 95%. SAXS and WAXS data was collected after every equilibration step which varied in length from 3 to 10 h.

Due to problems caused by an insufficient gas flow into the humidity chamber during the first adsorption sequence, leading to failure in keeping a constant RH at several points, the adsorption part of the experiment had to be remeasured. In this second experiment, the desorption cycle suffered from a technical error

© 2024 The Author(s). Small Structures published by Wiley-VCH GmbH

26884062, 2024, 12, Downloaded from https://onlinelibrary.wiley.com/doi/10.1002/sstr.202400167 by Aalto University, Wiley Online Library on [09/12/2024]. See the Terms and Conditions (https://onlinelibrary.wiley.com/terms-and-conditions) on Wiley Online Library for rules of use; OA articles are governed by the applicable Creative Commons License

in the humidity controller leading to an inability to reach very high or very low RH. This was fixed before the adsorption started. As confirmed gravimetrically (Section 2.4), these humidity fluctuations did not impact the samples in a significant way during the successful parts of the moisture cycle. Thus, the results of the successful parts of the two experiments were merged.

2.3.2. X-ray Scattering Data Analysis

Data Pre-treatment: The SAXS and WAXS intensities in the 2D scattering images were corrected for cosmic background and normalized based on transmitted beam intensity. After this, the background scattering, consisting of the empty sample holder measured at the corresponding RH, was removed. The wood samples produced strongly anisotropic scattering, leaving a part of the Kapton window contribution remaining at $q = 0.4\,\text{Å}^{-1}$. The thus obtained 2D patterns were corrected for solid angle to account for the rectangular detector geometry, as opposed to the ideal spherical geometry, and converted to polar representation using PyFAI.[14] Isotropic scattering was determined as the azimuthal minimum at each value of q by averaging the lowest 30% of values over the entire azimuthal profile. The equatorial scattering was calculated by azimuthally averaging 60° sectors, corresponding roughly to the entire width of the azimuthal scattering peak, along the equator perpendicular to the fiber axis, and then isotropic background was subtracted to arrive at the equatorial anisotropic scattering. This was done separately for SAXS and WAXS, and the resulting intensities were merged together into one 1D intensity curve. The same treatment was done for meriodional WAXS, in which case the anisotropic scattering was determined from 60° sectors parallel to the fiber axis. The resulting scattering intensity was multiplied by q to eliminate the effect of imperfect microfibril orientation.[15–18] This correction (Lorentz correction) and its effects are discussed in more detail in Section S3.5, Supporting Information. SAXS and WAXS data-analysis was done for scattering from delignified spruce and previously published data for untreated spruce[19] from the same tree using the same data pre-treatment.

Scattering Data Analysis by Fitting: Analyzing the equatorial anisotropic WAXS intensities was done by first subtracting a linear background between $q = 0.8 - 2.1\,\text{Å}^{-1}$. This q-range was chosen as it entirely contains the main equatorial reflections from cellulose I_β, while limiting overlap with the SAXS signal at lower q-values. After background subtraction, fitting was done with four Gaussian peaks which correspond to the $1\bar{1}0$, 110, and 200 (double peak) reflections of cellulose I_β. The 200 double peak consists of a broad and a narrow peak, and it is explained by a bimodal distribution of crystal sizes and allows a better fit than when using a single 200 peak[4] (see also Section S3.1, Supporting Information). The meridional anisotropic WAXS intensities were analyzed by fitting a constant background and a double peak between $q = 2.35 - 2.5\,\text{Å}^{-1}$, which corresponds to the 004 reflection, however only the more prominent peak was taken into account when calculating crystalline properties. The lattice spacing d_{hkl}, which corresponds to the interplanar distance between the (hkl) lattice planes in the microfibril was determined based on the peak location q_{hkl} and Bragg's law

$$d_{hkl} = \frac{2\pi}{q_{hkl}} \tag{1}$$

The coherence length of the crystalline order L_{hkl}, here referred to as "crystal size", in a direction perpendicular to the lattice plane (hkl) was calculated using the Scherrer equation[20,21]

$$L_{hkl} = \frac{2\pi}{\Delta q_{hkl}} \tag{2}$$

where Δq_{hkl} is the integral breadth of the fitted Gaussian. L_{hkl} increases when the crystal structure becomes more ordered and decreases when it becomes less ordered. In addition to determining the crystalline properties by peak fitting, also the proportion of crystalline material in the sample, here referred to as crystallinity index, and its changes in response to delignification and moisture were studied. The crystallinity index was calculated as a fraction of the integrated intensities from the equatorial crystalline $1\bar{1}0$, 110, and 200 peaks and the total scattering (further details in Section S3.6, Supporting Information).

SAXS arises from electron density contrast between different nanostructural components of the sample. In complex multicomponent materials like wood, the contrast conditions are not easy to determine. The following interpretation of the SAXS intensities is based on arguments derived from molecular modeling, which are presented later in Section 3.4. For scattering from the microfibrils, the highest contrast is between the fibril and the lignin/hemicellulose matrix including water. Removing lignin, which has an electron density higher than water, should affect the contrast between the remaining phases and thus the SAXS signal. Based on the molecular modeling results discussed later in Section 3.4 and 4, the sample was in all cases approximated as a two-phase system consisting of crystalline cellulose microfibrils and a matrix phase including the hemicelluloses, lignin, and water.

Due to substantial differences in the equatorial anisotropic SAXS intensities between the different samples and moisture conditions, different fitting strategies had to be selected depending on the case. The WoodSAS model[22] has been previously used to analyze small-angle scattering from cellulose microfibrils in wood. The model is as follows:

$$I(q) = AI_{\text{cyl}}(q, R, \Delta R, d_{\text{F}}, \Delta d_{\text{F}}) + Be^{-\frac{q^2}{2\sigma^2}} + Cq^{-\alpha} + I_{\text{BG}} \tag{3}$$

The A-term is based on hexagonally packed, infinitely long cylinders, corresponding to cellulose microfibrils and their packing and yields the mean fibril radius R, its polydispersity $\Delta R/R$, the fibril-to-fibril distance d_{F} and its polydispersity $\Delta d_{\text{F}}/d_{\text{F}}$. In this article, the symbol d_{F} is used instead of the a used in the original article.[22] The Gaussian B-term corresponding to slightly larger structures has no clear physical interpretation in SAXS, although it has been previously associated to bundles of microfibrils in small-angle neutron scattering.[23] The C-term represents Porod-scattering from surfaces of larger structures like the cell lumina. I_{BG} is a constant background.

The equatorial anisotropic SAXS intensities from untreated wood at RH 95% and below were fitted with the WoodSAS model of Equation (3) except that the B-term was not deemed necessary. SAXS data from the water-saturated delignified wood was fitted

© 2024 The Author(s). Small Structures published by Wiley-VCH GmbH

26884062, 2024, 12, Downloaded from https://onlinelibrary.wiley.com/doi/10.1002/sstr.202400167 by Aalto University, Wiley Online Library on [09/12/2024]. See the Terms and Conditions (https://onlinelibrary.wiley.com/terms-and-conditions) on Wiley Online Library for rules of use; OA articles are governed by the applicable Creative Commons License

using the *A*-term of the WoodSAS model with an additional single cylinder term, essentially another *A*-term where d_F was set arbitrarily high. Depending on the parameters of the single cylinders, radii of 1.3–2.3 nm and polydispersities of 0.1–0.4 resulted in reasonable fits when also accounting for the WoodSAS cylinder term. The results for the single cylinder fit are thus only given as a range of values. The interpretation of the additional cylinder term is discussed later in Section 3.3. Parameters $\Delta R/R = 0.22$ for the microfibrils and $\sigma = 0.065\,\text{Å}^{-1}$ were fixed, as done previously for untreated wood.[4]

Both water-saturated untreated wood and delignified wood at RH 95% and below showed a clear peak in the SAXS region, which was interpreted to arise from regular packing of the microfibrils. WoodSAS could not be fitted to the data due to the strong peak contribution, thus a simple model with a sum of a Gaussian function, a power-law, and a constant background was used to obtain the fibril-to-fibril distance d_F. These intensities were fitted using the equation:

$$I(q) = Aq^{-\alpha} + Be^{-\frac{(q-q_{SAXS})^2}{2\sigma^2}} + I_{BG} \tag{4}$$

where the location of the peak q_{SAXS} corresponds to a correlation distance between scattering structures, which then should roughly corresponds to the fibril-to-fibril distance d_F based on Bragg's law:

$$d_F \approx \frac{2\pi}{q_{SAXS}} \tag{5}$$

Examples of SAXS fits using the aforementioned models are shown later in Section 3.3. It must be noted that any value of d_F determined from scattering is an estimate based on a model and may not exactly equal the average physical distance between all the microfibrils due to local variations in the nanostructure and scattering contrast. The WoodSAS model, its compatibility with simple Gaussian fitting and the effects of multiplying the intensities by q are discussed in more detail in Section S3.5, Supporting Information.

2.4. Dynamic Vapor Sorption

Dynamic vapor sorption (DVS) was performed for three reasons: (1) to accurately determine the moisture content (MC) of the samples during the scattering experiments, (2) to confirm that the results from the two scattering experiments were compatible, and (3) to study the differences between the sorption behavior of untreated and delignified wood. Three cycles were investigated: following the first scattering experiment, following the second scattering experiment, and following an ideal experiment where the adsorption and desorption cycles worked as planned. For each DVS experiment, a never-dried piece of delignified spruce similar to the ones used in the scattering experiments was removed from deionized water, excess moisture was wiped from the surface, and the sample was placed inside the humidity and temperature-controlled sample environment of the DVS device (DVS ET, Surface Measurement Systems). Temperature was set to 25 °C and the RH was controlled to simulate each scattering experiment. Once the RH cycle was complete, RH was set to 0% and the sample was heated to 60 °C using the built-in heating coil for 6 h to completely dry the sample. The sample was then let equilibrate at RH 0% and 25 °C for 2 h to obtain the dry mass. The MC at each RH during the DVS measurement was calculated and used to estimate the MC during the scattering experiment. MC was defined as

$$\text{MC} = \frac{m_{water}}{m_{dry}} = \frac{m_{total} - m_{dry}}{m_{dry}} \tag{6}$$

where m_{total} is the mass of the sample at a given RH, m_{water} is the mass of water in the sample, and m_{dry} is the dry mass. The three DVS experiments confirmed that combining the successful desorption cycle of the first scattering experiment and the successful adsorption cycle of the second scattering experiment provided an MC at each RH that was consistent with an ideal continuous experiment, with the difference at any given RH being less than one percentage point.

2.5. Molecular Simulations

Molecular dynamics (MD) simulations were carried out to study the moisture response of lignin and cellulose–lignin interfaces within the cell wall nanostructure. The simulations address the effects of changing moisture content on 1) neat lignin and 2) aggregated microfibrils surrounded by lignin. The studied properties include volumetric swelling and contraction, distribution of bound water, and spatial density variation. The simulations are briefly described below, with further details given in Section S1, Supporting Information.

The neat lignin models were built by arranging 67 lignin chains of 25 monomeric units into a cubic simulation domain, along with different amounts of water, to obtain systems with MC between 0% and 25%. After the initial placement of the molecules, the systems were compressed into condensed phase models by a sequence of MD simulations. These include a heating step from room temperature to 500 K over 10 ns, an annealing step at 500 K over 100 ns, a cooling step back to room temperature over 100 ns, and a room temperature relaxation and sampling step over 200 ns. Data on water distribution and spatial density variation were gathered over the last 100 ns of the last simulation step. In addition, an isotropic scattering pattern was calculated from each trajectory. The chemical structure of the lignin molecules was based on the statistical description of spruce milled-wood lignin given by Balakshin et al.[24]

The microfibril aggregate models were built in several steps: 1) a model of an individual microfibril was cut from an equilibrated model of a bulk cellulose crystal; 2) the adsorption of galactoglucomannan (GGM) and glucuronoarabinoxylan (GAX) chains on the fibril surface was simulated in vacuum; 3) seven variants of the cellulose-hemicellulose fibril were arranged into a loose bundle with roughly 4 nm distance between the centers-of-mass of the fibrils; 4) the surrounding simulation domain was filled with lignin by using the neat lignin model at MC 20% as a structural template; 5) water was distributed in the system to obtain a model with an MC of roughly 40%. After the initial placement of the molecular components, the system was compressed into a condensed phase model by a sequence of MD simulations. These include a relaxation step for the water and lignin molecules at 500 K over 10 ns, a cooling step for

© 2024 The Author(s). Small Structures published by Wiley-VCH GmbH

26884062, 2024, 12, Downloaded from https://onlinelibrary.wiley.com/doi/10.1002/sstr.202400167 by Aalto University, Wiley Online Library on [09/12/2024]. See the Terms and Conditions (https://onlinelibrary.wiley.com/terms-and-conditions) on Wiley Online Library for rules of use; OA articles are governed by the applicable Creative Commons License

the same molecules from 500 K to room temperature over 1 ns, and a relaxation step for the whole system at room temperature over 10 ns. After the relaxation stage, the system was gradually dried using a protocol similar to that of Kulasinksi et al.[25] in which 10 water molecules were removed from the system between 100 ps simulations at room temperature. After each percentage-point drop in MC, a longer relaxation simulation of 1 ns was carried out. This resulted in a series of models with MC between 0 and 40%. A further relaxation and sampling simulation of 600 ns was carried out for each of the models. Data on water distribution and spatial density variation were gathered over the last 200 ns of this last simulation step. In addition, fibril-to-fibril distances and lattice spacings within the fibrils were determined. These analyses are described in detail in refs. [4,26]. The chemical structures of the GGM and GAX chains were chosen to mimic those found in softwood species.

The simulations were carried out using GROMACS[27] and the CHARMM carbohydrate[28,29] and lignin force fields.[30] The ParmEd,[31] doGlycans,[32] and LigninBuilder tools[33] were used for building the models. GROMACS utilities, MDAnalysis,[34,35] MDTraj,[36] and in-house software tools were used for trajectory analysis. The Debyer tool was used to calculate isotropic scattering patterns from the neat lignin trajectories.

3. Results

3.1. Raman Mapping Results

Confocal Raman microscopy allowed mapping the distribution and amount of lignin in the wood cells before and after delignification. The results are presented in **Figure 1**. Delignification reduced the Raman bands at 1151, 1271, 1456, 1601, 1663, 2939, and 3073 cm^{-1} (Figure 1a), which can be assigned to lignin.[37] The main lignin signal near 1600 cm^{-1} stems from vibration of the aromatic ring and was used to estimate the cellular distribution of lignin. The peak near 1600 cm^{-1} is believed to mainly come from the phenolic groups of lignin.[38] Since the peak had a clear decrease in all parts of the cell, the delignification was deemed successful.

The micrographs of untreated samples (Figure 1b,c) show the expected distribution of lignin: significant amounts in the middle lamellae, notable amounts in the cell wall, and no lignin in the lumen. Based on the reduction in band intensity of the main peak in the micrographs of the delignified sample, a delignification of 70–80% was reached within the cell walls, while an even greater reduction was seen in the cell corners. No noticeable change in the cellular morphology can be seen in the micrographs, indicating that delignification did not affect the cell structure in a significant manner.

3.2. DVS Results

The sorption curves for delignified wood, compared with those for untreated wood, are shown in **Figure 2**. The data for untreated spruce was obtained from Paajanen et al.[4] Delignified wood and untreated wood have almost identical MC at RH 85% and below, deviating from one another by less than 1 percentage point. However, at RH 95% delignified wood has more than 10 percentage points higher MC.

3.3. X-ray Scattering Results

X-ray scattering allows us to characterize wood nanostructure at various moisture conditions. By examining the differences and similarities in scattering between untreated and delignified wood at different moisture conditions, the impact of lignin on the cell wall structure and its moisture behavior can be investigated. Examples of 2D SAXS and WAXS patterns of untreated and delignified wood and 1D intensity curves derived from them are presented in **Figure 3**. The 2D patterns of both samples show similar strong preferred orientation, indicating that the orientation of the microfibrils along the fiber axis was roughly preserved in the delignification treatment. However, the untreated and delignified wood have otherwise noticeably different SAXS patterns in both 1D and 2D, indicating changes in the cell wall nanostructure.

In the 1D SAXS intensities, the delignified wood measured at RH 95% and below (Figure 3f) shows a much more prominent peak around $q = 0.15\ Å^{-1}$ than the untreated sample under the same conditions (Figure 3e). This implies that there is either a difference in the packing of microfibrils between the samples or that the lack of lignin introduces a significant change in the scattering length density contrast of the system as compared to untreated wood, or a combination of both effects. Based on model fitting to the equatorial anisotropic SAXS intensities of these samples (**Figure 4**a,b), the delignified wood had a clearly larger fibril-to-fibril distance d_F at all MCs (**Figure 5**).

The fibril-to-fibril distance in untreated wood is sensitive to moisture changes, increasing and decreasing reversibly with the MC of the cell wall.[4,10] As shown in Figure 5, this effect remains after delignification, but the relative and absolute magnitude of the change in d_F as a function of MC is smaller for delignified wood. Some of this difference is due to the different fitting methods illustrated in Figure 4a,b, due to which the d_F obtained by WoodSAS and the Gaussian peak fit differ at low MCs (see Figure S13, Supporting Information). However, the fitting method explains only part of the difference. Based on fitting the WoodSAS model to SAXS intensities of untreated and delignified wood without multiplying by q (Section S3.5, Supporting Information, especially Figure S11b and S13, Supporting Information), less than 50% of the difference in the behavior of d_F with respect to MC can be explained by the difference in fitting methods. This means that the smaller change in d_F in response to moisture changes in delignified wood is likely due to a real structural effect.

The changes due to delignification are much smaller in the WAXS range. Based on the fitting results (**Figure 6**), both the d_{200}-spacing and the coherence length of the crystalline order (crystal size) L_{200} are very similar between delignified and untreated wood. The 200 peak consisted of two overlapping peaks, a wide peak and a sharp peak which could be explained by a bimodal distribution of single and aggregated microfibrils,[4] respectively. Delignification seemed to increase the relative fraction of the sharp peak (Figure S6, Supporting Information) compared to the wide peak, suggesting slightly higher aggregation.

© 2024 The Author(s). Small Structures published by Wiley-VCH GmbH

26884062, 2024, 12, Downloaded from https://onlinelibrary.wiley.com/doi/10.1002/sstr.202400167 by Aalto University, Wiley Online Library on [09/12/2024]. See the Terms and Conditions (https://onlinelibrary.wiley.com/terms-and-conditions) on Wiley Online Library for rules of use; OA articles are governed by the applicable Creative Commons License

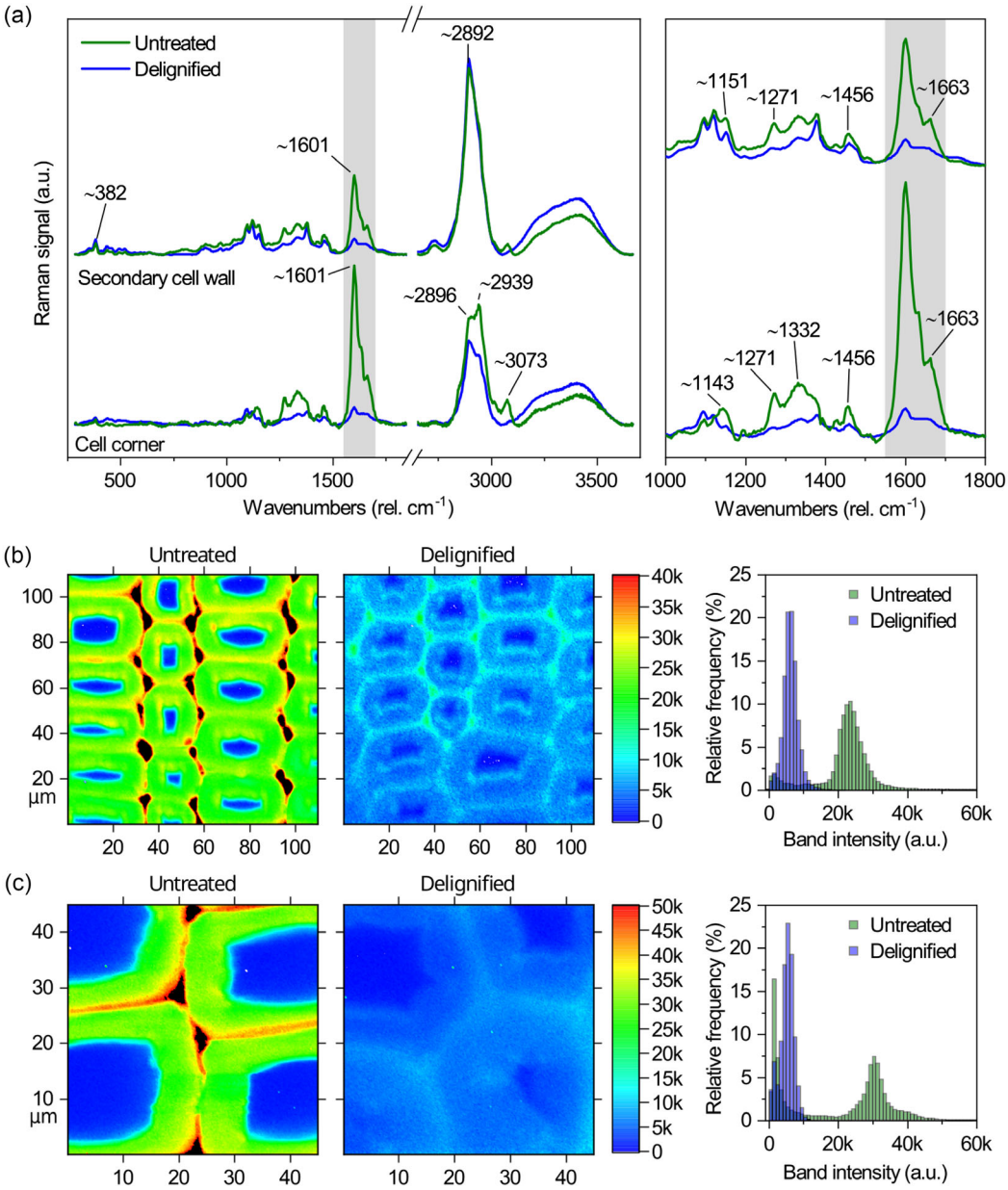

Figure 1. a) Raman spectra from both inside the secondary cell wall and at the cell corner (including the middle lamellae), with the most prominent lignin peak being highlighted for both untreated and delignified wood. b) Raman micrographs and corresponding pixel histograms based on the lignin signal at $1550 - 1700\ cm^{-1}$, taken with a 20× objective, along with a histogram of the total intensity of the lignin band. c) Same as (b) but with a 63× objective.

Also the crystalline properties d_{hkl} and L_{hkl} in the $[1\bar{1}0]$ and [110] directions (Figure S7, Supporting Information) show rather similar values in untreated and delignified wood, although fitting these peaks is prone to uncertainties. Qualitatively, the moisture response in the [110], $[1\bar{1}0]$, and [200] directions in the lateral cross-section of the microfibril is consistent between untreated and delignified wood, with little to no changes at higher MCs (>15%) and increasingly large changes when approaching MC 0% (increase in d_{200} and L_{110}, decrease in d_{110}, $d_{1\bar{1}0}$, L_{200}, and $L_{1\bar{1}0}$). This behavior has been previously explained by the deformation of cellulose crystals due to aggregation near the dry state.[4] The deformation is equal in magnitude in the untreated and delignified wood, despite the differences in the fibril-to-fibril distance (d_F), indicating that similar aggregated structures are present in both samples.

The [004] direction corresponds to the longitudinal structure along the cellulose chains. As seen in Figure 6 for both delignified and untreated wood, the d_{004} spacing remains relatively unaffected until low MCs, where it decreases slightly. For the crystal size L_{004}, the value at low MCs (<10%) was very similar between untreated and delignified wood. As MC increases, the L_{004} seems to grow faster for delignified wood. However, in our current data,

© 2024 The Author(s). Small Structures published by Wiley-VCH GmbH

26884062, 2024, 12, Downloaded from https://onlinelibrary.wiley.com/doi/10.1002/sstr.202400167 by Aalto University, Wiley Online Library on [09/12/2024]. See the Terms and Conditions (https://onlinelibrary.wiley.com/terms-and-conditions) on Wiley Online Library for rules of use; OA articles are governed by the applicable Creative Commons License

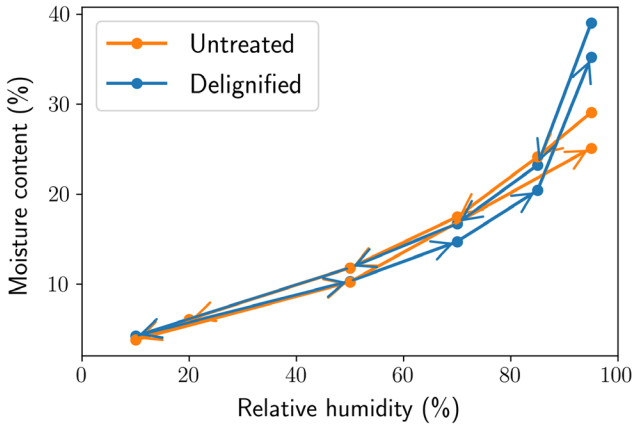

Figure 2. MC of the untreated and delignified wood samples as a function of RH, as measured using DVS. The desorption–adsorption cycle is shown with arrows. The data for untreated wood is from Paajanen et al.[4]

the 004 peak seemed to consist of two overlapping peaks like the 200 peak. For untreated wood, the two peaks seem to overlap more, while in the case of delignified wood, the peaks seem to slightly separate as the MC increases, indicating that the larger value of L_{004} for delignified wood compared to untreated wood at MC > 10% is somewhat unreliable. The data points on the q-axis at such high q-values were also sparse, leading to more uncertainty in the fitting. However, for both untreated and delignified wood, the L_{004} still seems to increase with MC in a similar manner. A hysteretic behavior with MC appears in the values of d_{004} in Figure 6, which results from the two separate scattering measurements of delignified wood (as explained in Section 2.3.1). The hysteresis was not present for the individual samples, or for any other property, which suggests that it is possibly caused by natural variation of the d_{004} lattice spacing between samples.[39]

The crystallinity index of the samples increased by 10 percentage points after delignification, from roughly 45% of the untreated wood to 55% (Figure S14, Supporting Information). Other than the increase in crystallinity between the two samples, the untreated and delignified sample behaved similarly with moisture, with crystallinity increasing as the sample dried, which can mostly be attributed to the removal of water (an amorphous component).

Clear differences due to delignification could be observed in the water-saturated samples. According to the results of SAXS fits to their equatorial anisotropic SAXS intensities (Figure 4c, d), the water-saturated samples had a larger fibril-to-fibril distance than those measured at RH 95% or below, and the values differed also due to delignification. For untreated water-saturated wood, the value $d_F = 5.2$ nm was obtained. In the water-saturated delignified wood, a large SAXS contribution in the q-range $0.02 - 0.2$ Å^{-1} (see also Figure 3f) made determining an exact value for d_F harder. Values of d_F between 6.0 and 7.5 nm provided the best fits, indicating that the fibril-to-fibril distance is likely larger in delignified wood than in untreated wood also in the water-saturated state. The WoodSAS fit of the water-saturated delignified wood also yielded fibril diameter

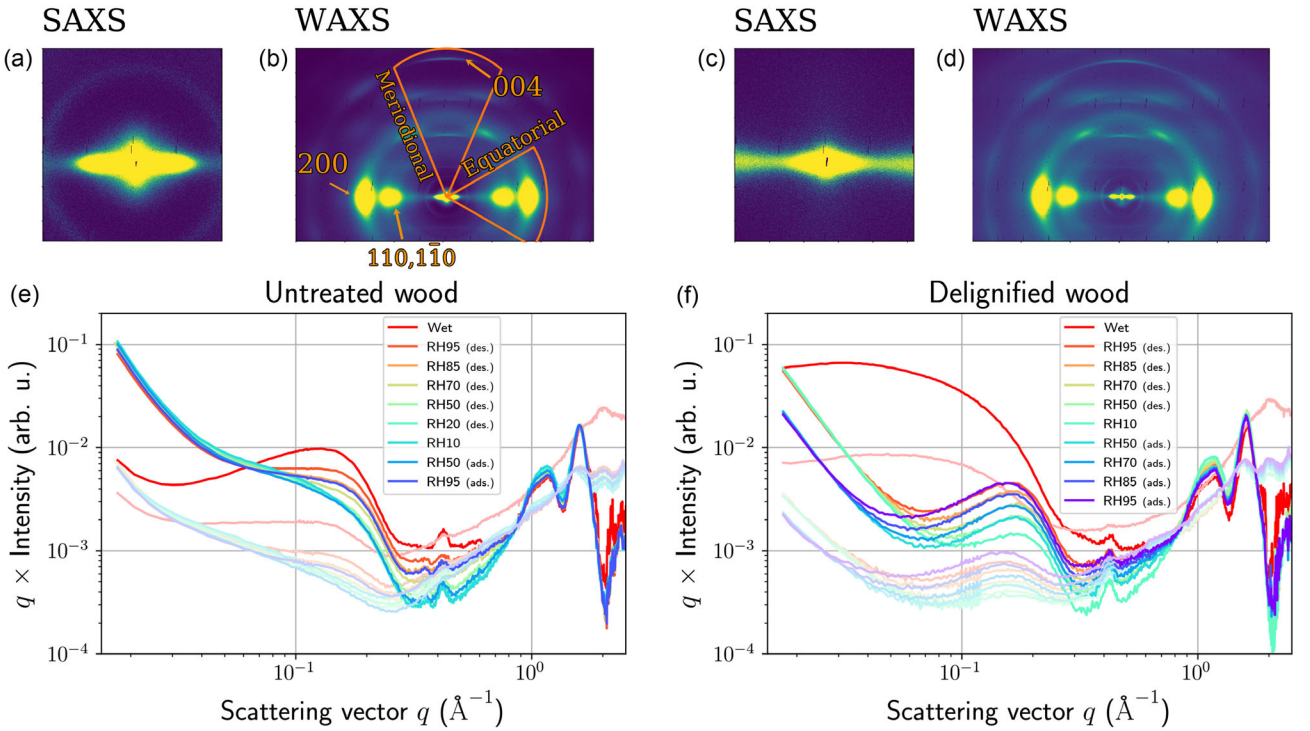

Figure 3. a) 2D SAXS and b) WAXS pattern from untreated wood. c) 2D SAXS and d) WAXS pattern from delignified wood. The patterns in (a) through (d) correspond to RH 50% during the desorption cycle. e) Combined 1D equatorial anisotropic SAXS/WAXS intensities from untreated wood at each RH. Isotropic scattering is shown with light-colored lines. f) Same as (e) but for delignified wood.

© 2024 The Author(s). Small Structures published by Wiley-VCH GmbH

26884062, 2024, 12, Downloaded from https://onlinelibrary.wiley.com/doi/10.1002/sstr.202400167 by Aalto University, Wiley Online Library on [09/12/2024]. See the Terms and Conditions (https://onlinelibrary.wiley.com/terms-and-conditions) on Wiley Online Library for rules of use; OA articles are governed by the applicable Creative Commons License

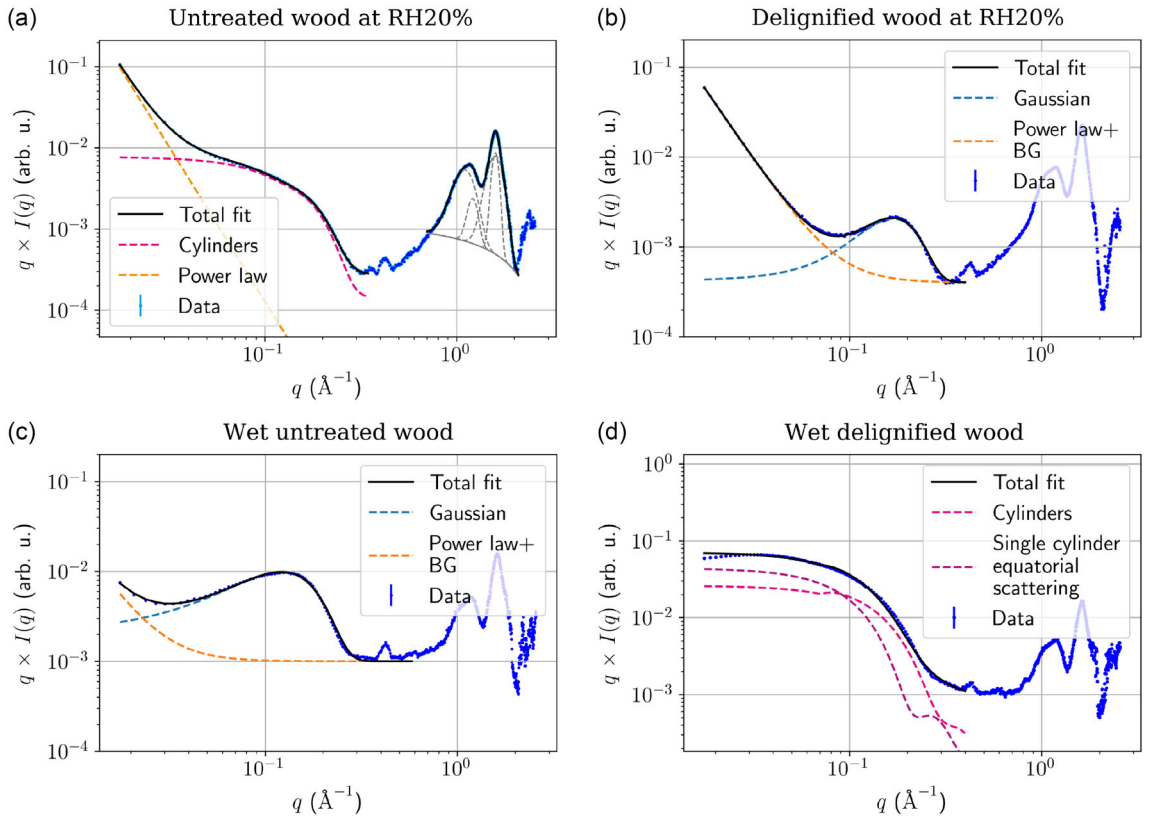

Figure 4. Equatorial anisotropic SAXS intensities and fits for delignified and untreated wood in both water-saturated and non-water-saturated states. a) Non-water-saturated untreated wood, fitted using Equation (3). Examples of the Gaussian peaks are shown in the WAXS region. b) Non-water-saturated delignified wood, fitted using Equation (4). c) Water-saturated untreated wood, fitted using Equation (4). d) Representative fit for water-saturated delignified wood, fitted using a combination of the WoodSAS cylinder term (*A*-term in Equation (3)) and a single cylinder equatorial scattering term.

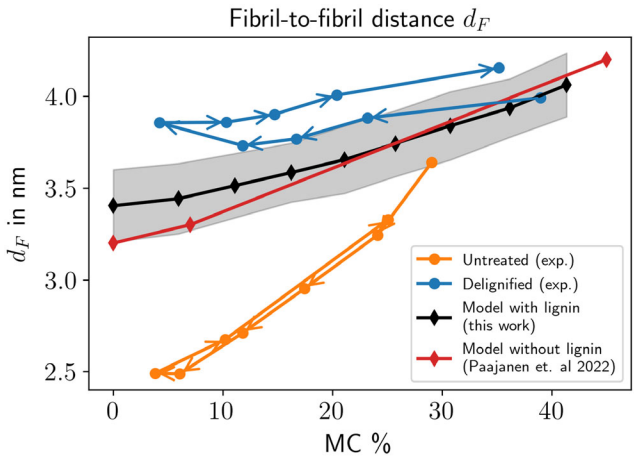

Figure 5. The fibril-to-fibril distance d_F determined from SAXS intensities for untreated and delignified wood. Also included are d_F values from the molecular model described in Section 2.5 and from a similar model that does not include lignin.[4] Desorption–adsorption cycle is indicated with arrows.

$2R$ and $\Delta d_F/d_F$ values similar with WoodSAS fits of the untreated wood samples at RH 95% and below. At the same time, the WAXS results show that the lattice spacings and crystal size were not significantly affected by increasing the MC over the MC at RH 95%. The parameters resulting from the scattering analysis of the water-saturated samples thus generally followed the same trends as observed for the samples at RH 95% and below.

In addition to the contribution from microfibrils, the dominating shoulder-like contribution at low q in the equatorial anisotropic SAXS intensity of water-saturated delignified wood was analyzed by fitting (Figure 4d). Using equatorial scattering from polydisperse single cylinders, this contribution was assigned to oriented structures with a cross-sectional diameter of ≈2.5–4.5 nm. Analyzing this feature of the SAXS intensity more accurately would benefit from a wider q-range as the intensity is still clearly changing toward the lowest detectable value of q. An alternative interpretation of the low-q scattering as a broad peak at $q = 0.035$ Å^{-1} would suggest some structure with an average packing distance of roughly 18 nm based on Bragg's law. Since the contribution only exists when the delignified wood is water-saturated and not when measured at RH 95% or below, it is likely that water makes the corresponding structures visible in SAXS either through changing the scattering length density contrast or causing a real change in the nanostructure. The cross-sectional diameter of 2.5–4.5 nm is roughly equal to the common size of nanoscale pores reported to exist in delignified wood[40,41] and a similar contribution was not seen in the SAXS

© 2024 The Author(s). Small Structures published by Wiley-VCH GmbH

26884062, 2024, 12, Downloaded from https://onlinelibrary.wiley.com/doi/10.1002/sstr.202400167 by Aalto University, Wiley Online Library on [09/12/2024]. See the Terms and Conditions (https://onlinelibrary.wiley.com/terms-and-conditions) on Wiley Online Library for rules of use; OA articles are governed by the applicable Creative Commons License

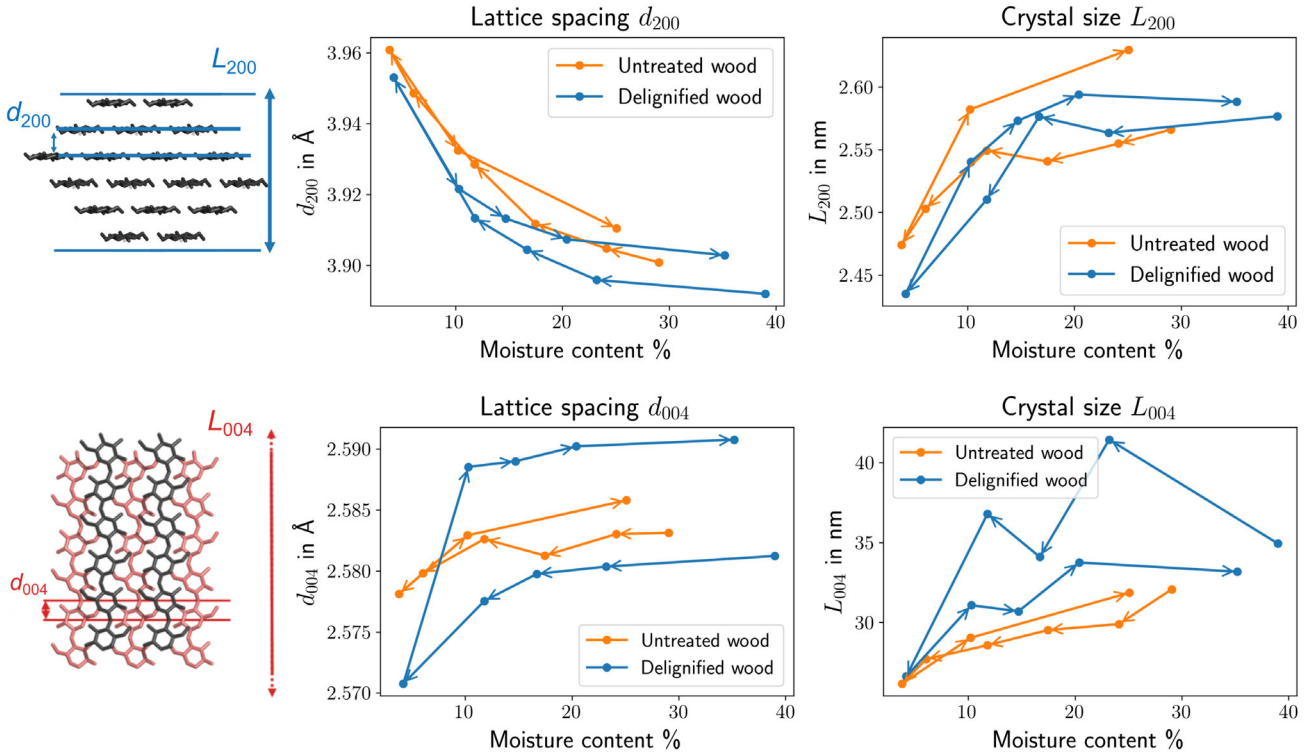

Figure 6. Lattice spacing d_{hkl} and the coherence length of crystalline order (crystal size) L_{hkl} for the [200] and [004] directions, based on fitting Gaussian peaks to the equatorial and meridional anisotropic WAXS intensities for untreated and delignified wood. Desorption–adsorption cycle is indicated with arrows.

intensities from untreated wood. It is possible that such pores collapse when water is removed from them, as has been seen in fully delignified wood.[9,41] Scattering methods are volume-averaging and thus cannot distinguish the exact location of the pores in the sample. However, as the signal from the assumed pores is strong when the wood is water-saturated, they likely occupy a significant volume fraction of the sample. It is therefore more likely that the pores are located throughout the cell wall than for example in the middle lamella, which make up only roughly 10% of the wood volume.[42] Thus, the SAXS contribution assigned to structures with a diameter estimated to be between 2.5 and 4.5 nm could be tentatively interpreted to arise from water-filled nanoscale pores in the cell walls, that close when the sample is dried to RH 95% or below.

The azimuthal distribution of the scattering intensity was also analyzed at various q-values, as shown in Figure S8, Supporting Information. Changes in the azimuthal distribution can be linked to changes in the orientation of the scattering structures, with wider profiles meaning less oriented structures. However, no noticeable changes were observed when comparing the azimuthal distributions from untreated and delignified wood. This indicates that the orientation distribution, including that of the cellulose microfibrils, was not significantly affected by the delignification. The water-saturated, delignified sample also showed no major difference compared to untreated wood. This indicates that the nanoscale pores were aligned in a similar manner to the microfibrils.

Besides the anisotropic equatorial and meridional scattering contributions, also the isotropic scattering visible in Figure 3e,f was examined. The isotropic scattering especially in delignified wood at RH 95% and below showed weak peaks at q-values that correspond roughly to the WAXS peaks of crystalline cellulose I_β, and a similar SAXS profile to the anisotropic equatorial scattering from cellulose microfibrils. This indicates that the isotropic scattering originates at least partially from cellulose microfibrils. These microfibrils are not well aligned along the fiber axis, which means that they could be located in other cell wall layers than the S2 layer of the secondary cell wall of tracheids, or in the walls of ray cells. The clear peak in the isotropic SAXS profile of delignified wood at RH 95% and below allowed fitting of a function that includes a Gaussian peak (Equation (4)) to determine the fibril-to-fibril distance d_F of the non-oriented microfibrils. The distance is almost equal to the anisotropic part, differing by at most 0.2 nm (see Figure S9, Supporting Information). Additionally, the moisture response of the unaligned fibrils seemed similar to the fibrils with preferred orientation along the fiber axis.

3.4. Molecular Simulation Results

Molecular modeling enables the study of cell wall nanostructure at a level of detail that is not accessible experimentally. These methods have been applied to cellulose-hemicellulose-lignin systems that mimic the cell wall structure with varying degrees of complexity and aim at explaining different aspects of its

© 2024 The Author(s). Small Structures published by Wiley-VCH GmbH

26884062, 2024, 12, Downloaded from https://onlinelibrary.wiley.com/doi/10.1002/sstr.202400167 by Aalto University, Wiley Online Library on [09/12/2024]. See the Terms and Conditions (https://onlinelibrary.wiley.com/terms-and-conditions) on Wiley Online Library for rules of use; OA articles are governed by the applicable Creative Commons License

behavior.[43–45] In the current work, the focus was on structural changes within a microfibril aggregate due to changing MC, the distribution of bound water, and the density contrast between the polysaccharide and lignin domains. Separate models were used to address the behavior of amorphous lignin without the presence of polysaccharide interfaces.

The model of a cellulose microfibril aggregate embedded in lignin displayed similar behavior to what was observed in the scattering experiments and previous models without lignin.[4,46] As the MC decreased, the initially separated fibrils approached each other and ultimately formed a closely-bound aggregate in the dry state. This is shown in **Figure 7** by model visualizations and in Figure 5 by the fibril-to-fibril distance. The lattice spacings in the [110], [1$\bar{1}$0], and [200] directions remained unaffected until an MC of roughly 10–15%, after which they began to increase with decreasing MC (Figure S5, Supporting Information). According to our interpretation presented in Paajanen et al.[4] these changes in the lattice spacings are due to the fibrils coming into direct contact with each other with the shrinking of the hemicellulose-water matrix, and the resulting formation of crystal-crystal interfaces. This does not apply to the [004] direction, where the lattice spacing decreased almost throughout the MC range, perhaps due to an influence of the contracting lignin matrix.

The simulations also predict how water is distributed within the system. As shown by the density maps in Figure 7, water preferred to occupy the inter-fibrillar region, forming a hemicellulose-water matrix around the fibrils. Water also resided within the lignin, but at a significantly lower concentration (the lignin-to-hemicellulose MC ratio was ≈2:5). At the same time, water was not able to penetrate crystalline cellulose regardless of the moisture environment. The findings made earlier are consistent with the common assumptions that water does not penetrate microfibril interiors and that it mainly interacts with the fibril surfaces and the hemicelluloses. Taken together, these observations suggest that, rather than spreading evenly in the structure, water is preferentially accumulated in the inter-fibrillar spaces as the cell wall MC increases.

The models of neat lignin (Figure S2, Supporting Information) displayed behavior that is characteristic of water adsorption into an amorphous polymer.[47–49] Starting from the dry state, the system could accommodate a small amount of water without notable volumetric swelling. This is evident from the increase in density when the MC increases from 0 to 5% (Figure S3a, Supporting Information). Above MC 5%, the system displayed a linear increase in volume with increasing MC, and a corresponding decrease in density. At the same time, the volume occupied by the added water would approach the specific volume of liquid water, which coincided with the formation and growth of water clusters. An increasing MC also resulted in an exponential increase in the water diffusivity. This behaviour has been linked to the growth of water-filled pores, and related decrease in the binding strength of water molecules at adsorption sites and in the complexity of their diffusion paths.[47]

Scattering intensities were computed from the neat lignin models to compare with the experimentally determined isotropic scattering from wood (Figure 3e,f). The lignin models produced a broad amorphous intensity distribution with a peak around $q = 1.5\ \text{Å}^{-1}$ (Figure S4, Supporting Information), which is consistent with experimentally measured scattering from lignin.[50] The peak in the computed scattering shifted toward higher q-values with increasing MC, which indicates a denser packing

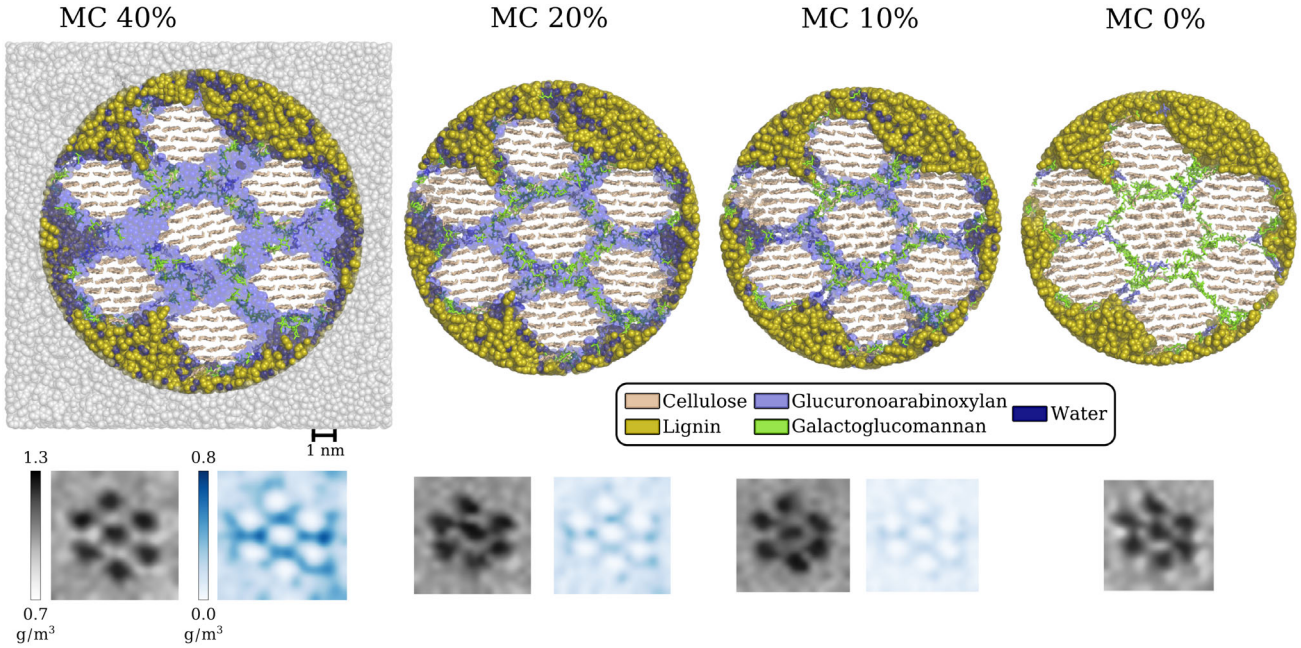

Figure 7. Visualization of the molecular model of a cellulose microfibril aggregate, shown at different MCs. The entire simulation domain is shown for the system with the most water (MC 40%). The cylindrical sub-system has a cellulose-hemicellulose-lignin mass ratio that corresponds to that of softwood secondary cell walls (roughly 2:1:1). The MC refers to that of the sub-system. In each case, color maps of the total mass (left) and water mass density (right) are shown below the simulation snapshot.

© 2024 The Author(s). Small Structures published by Wiley-VCH GmbH

26884062, 2024, 12, Downloaded from https://onlinelibrary.wiley.com/doi/10.1002/sstr.202400167 by Aalto University, Wiley Online Library on [09/12/2024]. See the Terms and Conditions (https://onlinelibrary.wiley.com/terms-and-conditions) on Wiley Online Library for rules of use; OA articles are governed by the applicable Creative Commons License

of lignin at the molecular level. Interestingly, a somewhat similar shift can be seen in the isotropic scattering from untreated wood and it is roughly reversible with changes in MC (Figure 3e and S4, Supporting Information). In the isotropic scattering from delignified wood (Figure 3f and S4, Supporting Information), the shift occurs only during desorption, indicating a possible irreversible change in the isotropic components of the nanostructure of delignified wood due to drying. This irreversibility may be related to the decrease in crystallinity index after the desorption-adsorption cycle that was observed only in the delignified wood (see Figure S14, Supporting Information). Moreover, the isotropic scattering intensity at $q = 0.5 - 1.5\,\text{Å}^{-1}$ measured from untreated wood shows higher values than that from delignified wood (Figure S4, Supporting Information), which coincides with the scattering computed from the lignin model and suggests that this excess contribution in untreated wood originates from lignin.

4. Discussion

Scattering methods were used to measure the changes caused by delignification in the nanostructure of spruce cell walls, as well as subsequent changes caused by varying MC. This was done both to understand the effects of delignification and to investigate indirectly the role of lignin in the moisture behavior of wood cell walls. Molecular simulations were used to support the experiments in describing the underlying phenomena. A summary of the proposed overall effects of delignification and drying are illustrated in **Figure 8**. Delignification (a → b in Figure 8) leads to regions formerly filled with lignin becoming available for water, which results in water-filled pores that are observable with SAXS in the water-saturated state. Regardless of the delignification, the cell wall structure contracts when dried (a → c and b → d in Figure 8), which is observed with SAXS as a reduction in the fibril-to-fibril distance d_F. The reduction in density due to delignification, while roughly preserving the sample dimensions (based on both of microscopic and macroscopic dimensional observations), might lead to more sparse fibril packing in the dry delignified cell walls as compared to those of untreated wood. However, based on the WAXS results, close aggregation of fibrils occurs in similar amounts in dry wood regardless of delignification.

According to our SAXS results, the main effect of delignification is the clear increase of the fibril-to-fibril distance d_F in both non-water-saturated (up to 1.2 nm, see Figure 5) and water-saturated wood (estimated to be 0.8–1.8 nm). Pine sawdust that has undergone an acid-chlorite treatment displayed a similar increase.[51] Wet, delignified birch also showed a similar increase (of 1.8 nm) as determined by small-angle neutron scattering.[52] Jungnikl et al.[53] found that their delignified wood made by a mild acid chlorite treatment did not exhibit a change in the SAXS profile or microfibril packing, but a harsher sodium hydroxide delignification caused a difference. It is clear that the method of delignification can have an impact on the fibril packing. The removal of lignin presumably allows some of the cellulose microfibrils to occupy regions previously containing lignin, resulting in a loosened fibrillar packing and an increase in d_F (as illustrated in Figure 8a → b). Contrary to the scattering results, in our molecular models, the presence of lignin has minimal impact on d_F when compared to a model without lignin (Figure 5). The main reasons for this likely come from how the

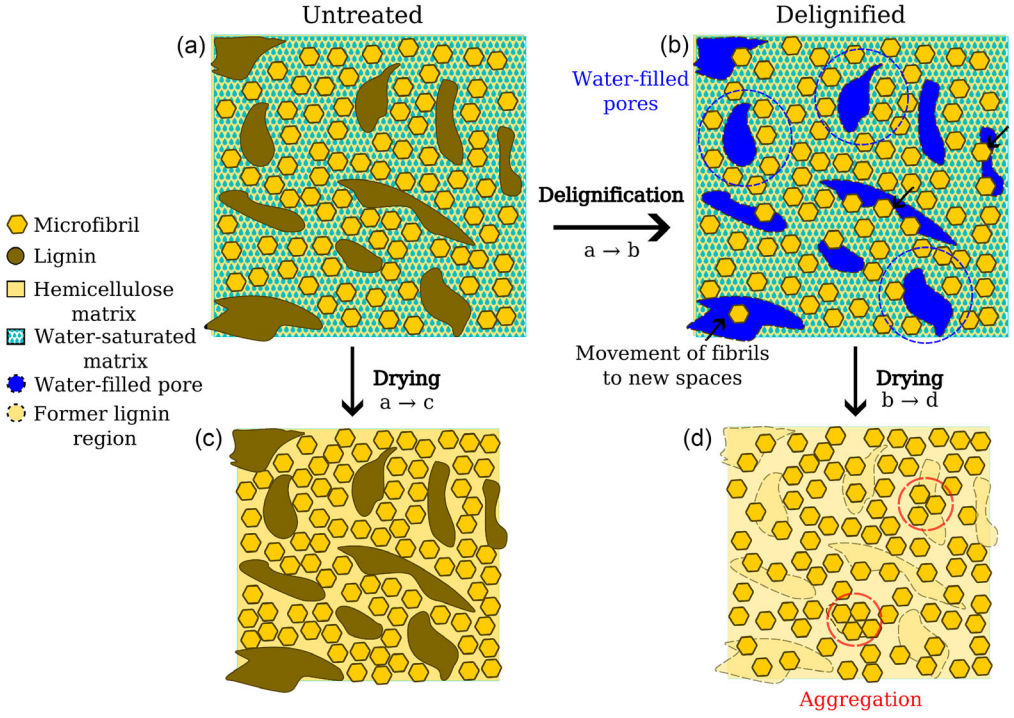

Figure 8. Proposed effects of drying and delignification on the cell wall properties. a) Water-saturated untreated wood, b) Water-saturated delignified wood, c) Dry untreated wood, and d) Dry delignified wood.

© 2024 The Author(s). Small Structures published by Wiley-VCH GmbH

26884062, 2024, 12, Downloaded from https://onlinelibrary.wiley.com/doi/10.1002/sstr.202400167 by Aalto University, Wiley Online Library on [09/12/2024]. See the Terms and Conditions (https://onlinelibrary.wiley.com/terms-and-conditions) on Wiley Online Library for rules of use; OA articles are governed by the applicable Creative Commons License

models were built. The hexagonal fibril bundle structure forces a specific kind of packing, and the surrounding lignin matrix can only affect it by changing how water is distributed across the system. Such an effect remains minimal due to preferential accumulation of water between the microfibrils. On the contrary, the difference in d_F between untreated and delignified wood detected by SAXS likely arises from larger, mesoscopic effects in the complex cell wall environment, where the presence or lack of lignin molecules can affect fibril packing and orientation at the level of structures larger than individual microfibril bundles.

Moisture behavior of the fibril packing was affected by delignification. In the experiments, a decrease in the change of d_F in response to moisture (both absolute and relative) is seen after delignification. The experimentally detected smaller change in d_F in response to moisture in delignified wood could be due to a lower packing density of the fibrils that should be a consequence of the approximately retained thickness of the cell wall after drying. This kind of effect would not be visible in molecular models built with the geometry adopted herein, and therefore in the models the presence of lignin has limited or no effect on the rate of change of d_F with MC. In contrast, the SAXS-based change in d_F with respect to MC in untreated wood would suggest much larger volumetric changes than those seen macroscopically. While swelling of the fibril structures and thus swelling of the cell wall is an important underlying cause in wood swelling, the swelling phenomenon is complex and occurs at multiple scales and cannot be attributed to microfibril bundle swelling alone. Additionally, due to the complex contrast environment and the approximations of the SAXS fitting method, the d_F may not represent the true average, which can lead to systematic deviations from the average physical distance between fibrils. Thus, the rate of change of d_F with MC shown for the models in Figure 5 seems more credible than that for the untreated wood based on SAXS, the difference being at least partially attributable to inaccuracies in the SAXS fitting results.

As determined by the DVS measurements (Figure 2), there is little difference in MC between untreated and delignified wood at RHs below 85%. However, above RH 85% the delignified wood adsorbs over 10 percentage points more water (in MC). Delignified wood reaching a larger MC at high RH has been observed before, and is likely due to a combination of three effects: the increased availability of sorption sites, lignin no longer constraining the swelling of the polysaccharide matrix and the formation of new pores and the expansion of existing ones.[5]

In water-saturated delignified wood, the SAXS intensities show a clear contribution that was interpreted to originate from aligned water-filled pores (Section 3.3), as illustrated in Figure 8b. The formation of pores in delignification has been studied in the past using water adsorption,[41] porosimetry,[54] gas adsorption[40,55] and atomic force microscopy.[56] As determined by SAXS, these pores have a cross-sectional diameter in the nanometer scale, with our estimates placing them in the 2.5–4.5 nm range. However, the SAXS fit at low-q (<0.04 Å^{-1}) is imprecise and a better fit would require data from lower values of q than was possible with the equipment used. To more accurately determine the mean pore size and the pore size distribution, methods such as ultra-small angle scattering would need to be used. Regardless, the contribution is still visible in our data and it is so large that it unlikely arises from microfibrils alone. No such contribution is present in untreated wood or less moist (below the fiber saturation point) delignified wood. According to our interpretation, this suggests that delignification creates pores with a characteristic cross-sectional size in the nanometer scale, and that the pores are visible in the SAXS range only when the cell wall is saturated by water. When the wood is dried below the fiber saturation point, for instance by equilibrating at RH 95%, the nanoscale pores presumably close and do not contribute to the SAXS intensity anymore. If they would remain open and empty, a SAXS contribution would be expected due to the strong density contrast.

The simulations provide a means to estimate the density contrast between cellulose microfibrils and their surroundings. This is relevant for the interpretation of SAXS results from complex multi-component materials like wood, because small-angle scattering arises from nanometer-level spatial variations in the scattering length density, which, in the case of SAXS, is proportional to electron density.[11] Based on the molecular models, both delignification and the presence of water strongly affect the density contrast of the system. In the models, the areas between the fibrils accommodate more water than the lignin domains, leading to a lower mass density of the interfibrillar spaces (Figure 7). The electron density difference between the hemicellulose-water matrix and the microfibril interior is therefore larger than that between the lignin-water matrix and the microfibril interior. This has two consequences for the scattering from the microfibrils: 1) a higher MC results in a higher contrast and stronger scattering since the fibrils are surrounded by more water, and 2) delignification results in a higher contrast and stronger scattering since the removal of the lignin regions leads to an increase in the relative amount of hemicellulose-water regions near the cellulose microfibrils. This improved contrast by increased MC and delignification probably accounts for some of the increasing SAXS peak intensity observed in the experiments (Figure 4). The molecular models also predict that the density difference between the fibrils and the lignin matrix, and between the fibrils and the hemicelluloses surrounding them, is sufficiently large to differentiate the microfibrils as separate entities even at low MC (Figure 7). These local density differences observed in the model at fully dry state are due to the formation of nanoscale voids in the inter-fibrillar space and at the cellulose–lignin interfaces. This would mean that there is enough contrast between the fibrils to make them always visible with SAXS, regardless of the MC. Therefore, it seems justifiable to interpret the SAXS results by assuming a two-phase system that consists of the cellulose microfibrils as one phase and the hemicellulose-lignin-water matrix as the other.

Our current models including lignin and previous modeling work without lignin[4] show very similar changes in the crystalline properties with respect to MC, with slight differences likely arising from a different force field rather than the presence of lignin. Such changes in crystal size L_{hkl} and lattice spacing d_{hkl} appear also in the experimental WAXS results for delignified and untreated wood. These properties remain essentially unaffected at higher MC and only start changing at low MC (Figure 6). Overall, the changes of the crystalline properties with respect to MC support the idea that crystal deformation due to aggregation of the fibrils happens at low MC, independent of the

© 2024 The Author(s). Small Structures published by Wiley-VCH GmbH

26884062, 2024, 12, Downloaded from https://onlinelibrary.wiley.com/doi/10.1002/sstr.202400167 by Aalto University, Wiley Online Library on [09/12/2024]. See the Terms and Conditions (https://onlinelibrary.wiley.com/terms-and-conditions) on Wiley Online Library for rules of use; OA articles are governed by the applicable Creative Commons License

presence of lignin.[4] While a considerable portion of the fibrils in delignified wood are too far from each other as indicated by the large fibril-to-fibril distance from SAXS, local aggregation is still possible. It can be speculated that delignification both aids fibril aggregation by removing lignin molecules that could prevent fibrils from approaching each other and impedes it by creating more space and increasing the distance between some microfibrils. This is shown in Figure 8c,d, where the average distance between fibrils after delignification is larger but new aggregation possibilities also become available. Due to the changes in crystalline properties with respect to moisture being roughly the same for untreated and delignified wood, it seems that roughly the same amount of fibril aggregates exist in both untreated and delignified wood. This means that either already aggregated fibrils within the cell wall remain as aggregated as before delignification and/or new aggregates form during delignification, preserving the aggregation-related WAXS behavior similar despite an overall increase in d_F. This suggests that less aggregated fibrils are responsible for the increase in d_F.

5. Conclusions

We studied the effects of delignification on wood nanostructure and moisture behavior using scattering methods and molecular simulations. The delignification increased the distance between cellulose microfibrils, which is likely caused by the increased availability of space within the cell wall nanostructure after the removal of lignin. Also aligned water-filled pores were formed between the microfibril bundles. According to both the experimental SAXS and WAXS results and the molecular modeling, the presence or absence of lignin did not affect the underlying phenomena responsible for moisture-induced swelling of microfibril bundles and the behavior of crystalline cellulose with moisture.

Supporting Information

Supporting Information is available from the Wiley Online Library or from the author.

Acknowledgements

This work was a part of the Research Council of Finland's Flagship Programme under Projects No. 318890 and 318891 (Competence Center for Materials Bioeconomy, FinnCERES). P.A.P. thanks the Research Council of Finland for funding (grant nos. 338804 and 359121). M.A. and L.R. thank the Research Council of Finland for funding (grant no. 341701). The authors wish to acknowledge CSC – IT Center for Science, Finland, for computational resources. This work made use of Aalto University's Bioeconomy Facilities and OtaNano–Nanomicroscopy Center Facilities.

Conflict of Interest

The authors declare no conflict of interest.

Data Availability Statement

The data that support the findings of this study are available from the corresponding author upon reasonable request.

Keywords

lignin, moisture interactions, molecular dynamics, wood nanostructure, X-ray scattering

Received: April 8, 2024
Revised: July 9, 2024
Published online: October 28, 2024

[1] E. T. Engelund, L. G. Thygesen, S. Svensson, C. A. S. Hill, *Wood Sci. Technol.* **2012**, *47*, 141.
[2] E. E. Thybring, M. Fredriksson, S. L. Zelinka, S. V. Glass, *Forests* **2022**, *13*, 2051.
[3] O. M. Terrett, P. Dupree, *Curr. Opin. Biotechnol.* **2019**, *56*, 97.
[4] A. Paajanen, A. Zitting, L. Rautkari, J. A. Ketoja, P. A. Penttilä, *Nano Lett.* **2022**, *22*, 5143.
[5] T. Yang, J. Cao, C. Mei, E. Ma, *Cellulose* **2021**, *28*, 9461.
[6] D. Huang, R. Li, P. Xu, T. Li, R. Deng, S. Chen, Q. Zhang, *Chem. Eng. J.* **2020**, *402*, 126237.
[7] T. Yang, D. Luo, C. Hu, L. Wang, C. Mei, *Wood Mater. Sci. Eng.* **2023**, *3*, 580.
[8] J. Li, C. Chen, J. Y. Zhu, A. J. Ragauskas, L. Hu, *Acc. Mater. Res.* **2021**, *2*, 606.
[9] A. Kumar, T. Jyske, M. Petrič, *Adv. Sustainable Syst.* **2021**, *5*, 5.
[10] N. Z. Plaza, S. V. Pingali, S. Qian, W. T. Heller, J. E. Jakes, *Cellulose* **2016**, *23*, 1593.
[11] P. A. Penttilä, A. Paajanen, J. A. Ketoja, *Carbohydr. Polym.* **2021**, *251*, 117064.
[12] C. Schuerch, *J. Polym. Sci., Part A-2: Polym. Phys.* **1968**, *6*, 394.
[13] P. A. Ahlgren, D. A. I. Goring, *Can. J. Chem.* **1971**, *49*, 1272.
[14] J. Kieffer, V. Valls, N. Blanc, C. Hennig, *J. Synchrotron Radiat.* **2020**, *27*, 558.
[15] T. Hashimoto, T. Kawamura, M. Harada, H. Tanaka, *Macromolecules* **1994**, *27*, 3063.
[16] J. Samon, J. Schultz, B. Hsiao, *Polymer* **2000**, *41*, 2169.
[17] A. Sharma, P. Wankhede, R. Samant, S. Nagarkar, S. Thakre, G. Kumaraswamy, *ACS Appl. Polym. Mater.* **2021**, *3*, 2598.
[18] T. Kuribayashi, Y. Ogawa, I. Morfin, Y. Matsumoto, Y. Nishiyama, *Cellulose* **2023**, *30*, 8405.
[19] P. Penttilä, A. Zitting, *X-ray Scattering Data From Norway Spruce at Different Moisture Conditions*, Zenodo **2022**, https://zenodo.org/record/6557385.
[20] J. I. Langford, A. J. C. Wilson, *J. Appl. Crystallogr.* **1978**, *11*, 102.
[21] P. Scardi, M. Leoni, R. Delhez, *J. Appl. Crystallogr.* **2004**, *37*, 381.
[22] P. A. Penttilä, L. Rautkari, M. Österberg, R. Schweins, *J. Appl. Crystallogr.* **2019**, *52*, 369.
[23] P. A. Penttilä, M. Altgen, M. Awais, M. Österberg, L. Rautkari, R. Schweins, *Sci. Rep.* **2020**, *10*, 20844.
[24] M. Balakshin, E. A. Capanema, X. Zhu, I. Sulaeva, A. Potthast, T. Rosenau, O. J. Rojas, *Green Chem.* **2020**, *22*, 3985.
[25] K. Kulasinski, R. Guyer, D. Derome, J. Carmeliet, *Biomacromolecules* **2015**, *16*, 2972.
[26] A. Zitting, A. Paajanen, P. A. Penttilä, *Cellulose* **2023**, *30*, 8107.
[27] M. J. Abraham, T. Murtola, R. Schulz, S. Páll, J. C. Smith, B. Hess, E. Lindahl, *SoftwareX* **2015**, *1*, 19.

© 2024 The Author(s). Small Structures published by Wiley-VCH GmbH

26884062, 2024, 12, Downloaded from https://onlinelibrary.wiley.com/doi/10.1002/sstr.202400167 by Aalto University, Wiley Online Library on [09/12/2024]. See the Terms and Conditions (https://onlinelibrary.wiley.com/terms-and-conditions) on Wiley Online Library for rules of use; OA articles are governed by the applicable Creative Commons License

[28] O. Guvench, E. Hatcher, R. M. Venable, R. W. Pastor, A. D. MacKerell, *J. Chem. Theory Comput.* **2009**, *5*, 2353.
[29] E. P. Raman, O. Guvench, A. D. MacKerell, *J. Phys. Chem. B* **2010**, *114*, 12981.
[30] J. V. Vermaas, L. Petridis, J. Ralph, M. F. Crowley, G. T. Beckham, *Green Chem.* **2019**, *21*, 109.
[31] M. R. Shirts, C. Klein, J. M. Swails, J. Yin, M. K. Gilson, D. L. Mobley, D. A. Case, E. D. Zhong, *J. Comput.-Aided Mol. Des.* **2017**, *31*, 147.
[32] R. Danne, C. Poojari, H. Martinez-Seara, S. Rissanen, F. Lolicato, T. Róg, I. Vattulainen, *J. Chem. Inf. Model.* **2017**, *57*, 2401.
[33] J. V. Vermaas, L. D. Dellon, L. J. Broadbelt, G. T. Beckham, M. F. Crowley, *ACS Sustainable Chem. Eng.* **2019**, *7*, 3443.
[34] R. Gowers, M. Linke, J. Barnoud, T. Reddy, M. Melo, S. Seyler, J. Domanski, D. Dotson, S. Buchoux, I. Kenney, O. Beckstein, in *MDAnalysis*, SciPy **2016**, pp. 98–105, https://conference.scipy.org/proceedings/scipy2016/oliver_beckstein.html.
[35] N. Michaud-Agrawal, E. J. Denning, T. B. Woolf, O. Beckstein, *J. Comput. Chem.* **2011**, *32*, 2319.
[36] R. T. McGibbon, K. A. Beauchamp, M. P. Harrigan, C. Klein, J. M. Swails, C. X. Hernández, C. R. Schwantes, L.-P. Wang, T. J. Lane, V. S. Pande, *Biophys. J.* **2015**, *109*, 1528.
[37] U. P. Agarwal, J. D. McSweeny, S. A. Ralph, *J. Wood Chem. Technol.* **2011**, *31*, 324.
[38] U. P. Agarwal, R. H. Atalla, *Planta* **1986**, *169*, 325.
[39] L. H. Thomas, C. M. Altaner, V. T. Forsyth, E. Mossou, C. J. Kennedy, A. Martel, M. C. Jarvis, *Sci. Rep.* **2021**, *11*, 453.
[40] J. Yin, K. Song, Y. Lu, G. Zhao, Y. Yin, *Wood Sci. Technol.* **2015**, *49*, 987.
[41] P. Grönquist, M. Frey, T. Keplinger, I. Burgert, *ACS Omega* **2019**, *4*, 12425.
[42] B. J. Fergus, A. R. Procter, J. A. N. Scott, D. A. I. Goring, *Wood Sci. Technol.* **1969**, *3*, 117.
[43] K. Kulasinski, D. Derome, J. Carmeliet, *J. Mech. Phys. Solids* **2017**, *103*, 221.
[44] C. Zhang, M. Chen, S. Keten, B. Coasne, D. Derome, J. Carmeliet, *Sci. Adv.* **2021**, *7*, eabi8919.
[45] D. Sarkar, L. Bu, J. E. Jakes, J. K. Zieba, I. D. Kaufman, M. F. Crowley, P. N. Ciesielski, J. V. Vermaas, *Cell Surf.* **2023**, *9*, 100105.
[46] A. Zitting, A. Paajanen, P. A. Penttilä, L. Rautkari, *Cellulose* **2021**, *28*, 10765.
[47] K. Kulasinski, R. Guyer, D. Derome, J. Carmeliet, *Langmuir* **2015**, *31*, 10843.
[48] K. Kulasinski, L. Salmén, D. Derome, J. Carmeliet, *Cellulose* **2016**, *23*, 1629.
[49] C. Zhang, A. Shomali, R. Guyer, S. Keten, B. Coasne, D. Derome, J. Carmeliet, *Macromolecules* **2020**, *53*, 1527.
[50] P. Ahvenainen, I. Kontro, K. Svedström, *Cellulose* **2016**, *23*, 1073.
[51] X. Miao, W. Hua, Y. Li, F. Bian, T. Xiao, *Heliyon* **2024**, *10*, e25355.
[52] P. Chen, Y. Li, Y. Nishiyama, S. V. Pingali, H. M. O'Neill, Q. Zhang, L. A. Berglund, *Nano Lett.* **2021**, *21*, 2883.
[53] K. Jungnikl, O. Paris, P. Fratzl, I. Burgert, *Cellulose* **2007**, *15*, 3.
[54] S. Vitas, J. Segmehl, I. Burgert, E. Cabane, *Materials* **2019**, *12*, 416.
[55] T. Nakatani, Y. Ishimaru, I. Iida, Y. Furuta, *J. Wood Sci.* **2008**, *54*, 252.
[56] M. Adobes-Vidal, M. Frey, T. Keplinger, *J. Struct. Biol.* **2020**, *211*, 107532.

© 2024 The Author(s). Small Structures published by Wiley-VCH GmbH

26884062, 2024, 12, Downloaded from https://onlinelibrary.wiley.com/doi/10.1002/sstr.202400167 by Aalto University, Wiley Online Library on [09/12/2024]. See the Terms and Conditions (https://onlinelibrary.wiley.com/terms-and-conditions) on Wiley Online Library for rules of use; OA articles are governed by the applicable Creative Commons License